



Article

Dynamic Behavior Forecast of an Experimental Indirect Solar Dryer Using an Artificial Neural Network

Angel Tlatelpa Becerro ^{1,*}, Ramiro Rico Martínez ^{2,*}, Erick César López-Vidaña ³, Esteban Montiel Palacios ⁴, César Torres Segundo ⁴ and José Luis Gadea Pacheco ⁴

¹ Departamento de Ingeniería en Robótica y Manufactura Industrial, Escuela de Estudios Superiores de Yecapixtla, Universidad Autónoma del Estado de Morelos, Yecapixtla 62824, Mexico

² Tecnológico Nacional de México, I.T. Celaya, Celaya 38000, Mexico

³ Consejo Nacional de Humanidades, Ciencias y Tecnología, Centro de Investigación en Materiales Avanzados S.C., Durango 34147, Mexico; erick.lopez@cimav.edu.mx

⁴ Escuela de Estudios Superiores de Xalostoc, Universidad Autónoma del Estado de Morelos, Ayala 62725, Mexico; esteban.montiel@uaem.mx (E.M.P.); cesar.torres@uaem.mx (C.T.S.); jose.gadea@uaem.mx (J.L.G.P.)

* Correspondence: angel.tlatelpa@uaem.mx (A.T.B.); ramiro@iqcelaya.itc.mx (R.R.M.)

Abstract: This research presents the prediction of temperatures in the chamber of a solar dryer using artificial neural networks (ANN). The dryer is a forced-flow type and indirect. Climatic conditions, temperatures, airflow, and geometric parameters were considered to build the ANN model. The model was a feed-forward network trained using a backpropagation algorithm and Levenberg–Marquardt optimization. The configuration of the optimal neural network to carry out the verification and validation processes was nine neurons in the input layer, one in the output layer, and two hidden layers of thirteen and twelve neurons each (9-13-12-1). The percentage error of the predictive model was below 1%. The predictive model has been successfully tested, achieving a predictor with good capabilities. This consistency is reflected in the relative error between the predicted and experimental temperatures. The error is below 0.25% for the model’s verification and validation. Moreover, this model could be the basis for developing a powerful real-time operation optimization tool and the optimal design for indirect solar dryers to reduce cost and time in food-drying processes.

Keywords: solar dryer; thermal analysis; electronic instrumentation; artificial neural networks; feedforward propagation algorithm



Citation: Tlatelpa Becerro, A.; Rico Martínez, R.; López-Vidaña, E.C.; Montiel Palacios, E.; Torres Segundo, C.; Gadea Pacheco, J.L. Dynamic Behavior Forecast of an Experimental Indirect Solar Dryer Using an Artificial Neural Network. *AgriEngineering* **2023**, *5*, 2423–2438. <https://doi.org/10.3390/agriengineering5040149>

Academic Editors: Ray E. Sheriff and Chiew Foong Kwong

Received: 26 October 2023

Revised: 1 December 2023

Accepted: 8 December 2023

Published: 14 December 2023



Copyright: © 2023 by the authors. Licensee MDPI, Basel, Switzerland. This article is an open access article distributed under the terms and conditions of the Creative Commons Attribution (CC BY) license (<https://creativecommons.org/licenses/by/4.0/>).

1. Introduction

Developing dehydrated vegetable and meat products has gained economic importance worldwide to preserve food and increase its shelf life. Drying is one of the oldest and most used techniques for food preservation [1]. Its function is to eliminate the water that contains the food, which inhibits the proliferation of microorganisms and hinders putrefaction. However, many processes are based on artisan techniques, which provide poor quality and repeatability in the resulting products. Nevertheless, the globalization trend has aroused interest in increasing its production, controlling the quality of its products, and expanding its offerings by accelerating the drying processes, seeking to add value to “artisanal” products [2].

Furthermore, there is a vision of sustainable development for food preservation, which is sought to be supported by using renewable energies, such as solar energy, both for artisanal and industrial processes [3,4].

Based on this perspective, solar drying through solar dryers is an attractive process for food dehydration applications [5]. Some solar dryers are considered direct because the foods are exposed to radiation [1], and they use a black surface to increase the air temperature to dry the product. Indirect solar dryers, on the other hand, comprise the

solar collector and the drying chamber, and the solar radiation does not affect the products' surface; this equipment's performance can be by natural or forced convection. For this configuration, the collector receives solar radiation to increase the airflow temperature supplied through it, and the chamber is where the air circulates to remove moisture from the product. This system is desirable as it does not require high temperatures, exhibits greater drying efficiency, and does not require energy storage because the temperature required for drying fruits and vegetables is between 30 and 70 °C [1] and because it manages to reach these temperatures. However, these devices operate in areas with abundant solar radiation and climatic conditions, such as those in tropical regions, under semi-cloudy and clear-sky conditions.

In this study, an experimental forced-flow indirect solar dryer is used for research purposes. This system is considered complex for its geometry and operating principle since its performance depends on weather conditions. It requires a system to supply airflow that guarantees adequate air circulation.

The design, development, and analysis of the thermal behavior of solar dryers have been widely studied theoretically with numerical analysis and experimental studies. For numerical analysis, computational fluid dynamics (CFD) was used to analyze heat and mass transfer to determine the behavior of temperatures, flows, and moisture loss in the dryers [6–8]. In experimental studies, dryers were instrumented to monitor the behavior of temperatures, airflows, and moisture and the data compared with computational numerical simulations to validate their models [3,9–11]. On the other hand, different methodologies have been applied to obtain mathematical models and numerically simulate dryers to describe their performance [12,13]. For these study cases, it has been found that moisture tends to decrease when the temperature increases inside the drying chamber. This improves the equipment's performance in drying food. However, each of these papers aims to determine a design that allows the ideal temperature inside the drying chamber to be obtained by evaluating thermal performance by applying mathematical models, numerical computational simulations, and experimental studies.

The ideal conditions in a solar dryer allow for calculating the drying kinetics of products such as vegetables, meats, and other materials [4,12–16]. Due to the system's complexity, it is difficult to determine the performance of the solar dryer. Moreover, the techniques used become tedious and computationally expensive. Looking for new practical alternatives to predict the air temperature inside the chamber of a solar dryer to improve the designs and optimize the operation is a challenge. One of the computational models that impact a predictive analysis tool in thermal systems is the artificial neural networks (ANN) technique.

This technique consists of models inspired by the biology of the human brain [17]. It offers an alternative to solving complex problems in real situations. Otherwise, it would be tough to characterize using analytical techniques and numerical simulation since they do not require detailed knowledge of the physical phenomena of thermal systems [18]. Recently, ANNs have been used in different engineering fields in pattern recognition, adaptive control systems, and complex thermal systems [19–21]. They have been applied to modeling and predicting thermal performance in heat pumps for cooling and heating [18,22,23] and performing modeling in reactors for storing sorption energy to predict the dynamics of charge and temperature state [24]. Likewise, neural networks have been applied to simulate solar collectors' thermal performance and calculate solar radiation [25–28].

Similarly, studies have been carried out in heat exchangers for the predictive analysis of heat transfer, pressure drop, and control [20,29–33]. Also, this technique has been used to predict temperatures and mass flow and calculate thermal behavior in heat exchangers [34–36]. It has been applied to describe fluidized bed dryers, predicting the drying characteristics of potatoes, garlic, and melon [37] and microwave-assisted green pea-drying time prediction [38]. Likewise, predictions have been made to calculate the moisture content in wheat [39]. Also, ANNs have worked on modeling the performance of a parabolic greenhouse dryer for drying lychee pulp [40].

This research presents the prediction of temperatures in the chamber of a solar dryer using artificial neural networks (ANN). The dryer under study is indirect and forced flow. It comprises a solar collector and a drying chamber with trays for food. The objective is to build a predictive model of the temperature of the drying chamber. For this purpose, solar radiation and ambient temperature are considered, as well as the temperatures of the pipes and the speed of the airflow inside the drying chamber. A model dryer was instrumented with temperature sensors, an airflow meter, and a meteorological station for climate conditions for experimental purposes. The latter were recorded with an Arduino-type microcontroller and LabVIEW Student Software Suite 2020, respectively. Also, the number and spacing of trays were considered. The proposed artificial neural network model was applied to model the system and validated with experimental data. This network model could be a powerful tool to assist in the design of solar dryers as well as the optimization of their operation.

2. Materials and Methods

The study of solar dryers remains a complex problem. Different innovative proposals in the literature combine theoretical, numerical, and experimental procedures for thermal analysis. However, only some of them are suitable for online applications. In some cases, the analysis is limited to the effect of the internal geometry of the dryer on its dynamic behavior. For this reason, this research paper proposes using artificial neural networks to predict the air temperature inside the drying chamber for different numbers and positions of trays inside the dryer chamber.

This section describes the experimental solar dryer in detail, then the electronic communication between a microcontroller and the LabVIEW Student Software Suite 2020 for applied electronic instrumentation and practical data acquisition. Finally, artificial neural networks are presented to predict the state of the solar dryer.

2.1. Experimental Setup of the Solar Dryer

This experimental work was developed in Yecapixtla, Morelos, Mexico, at $18^{\circ}51'09.6''$ north latitude and $98^{\circ}52'11.0''$ west longitude. The solar dryer is outdoors and faces south for maximum use of solar energy. The collector has a tilt angle of 24° and the following dimensions: length (L_1) 2.145 m, width (W_1) 0.95 m, and height (D_1) 0.13 m, and for the chamber, the following: height (L_2) 1.27 m, width (W_2) 1.0 m, and depth (D_2) 0.455 m (Figure 1a). The solar collector comprises three parts: a 20-gauge stainless steel casing; an arrangement of sixteen copper ducts with dimensions of 1.5 m in length, an external diameter of 0.0266 m, and a 0.001 cell for airflow passage; and lastly, a clear acrylic cover. The main component of the collector is the energy-absorbing pipes. These are painted matte black to absorb and take advantage of the most remarkable solar radiation available during the day.

The underside and the sides are insulated to minimize heat loss. The thermal insulation is a 3 cm thick polyurethane foam between the housing and a reflective aluminum sheet. The clear acrylic cover reduces convection heat loss from the absorber pipes. The air inlet to the collector is in the lower part (Color blue arrows), and the air outlet in the upper (Color yellow arrows) part connects to the drying chamber (Figure 1b). The airflow that enters the collector passes into the ducts, raises the temperature, and is transported to the drying chamber. The drying chamber is constructed of stainless steel and painted matte black to absorb radiant energy and increase indoor air temperature. The airflow that enters the chamber is in the lower part (Color yellow arrows), and the outlet (Color green arrows) is in the upper part (Figure 1c). The drying chamber contains spaces for a maximum of fifteen mobile trays. The trays are used to dehydrate or dry a product. For this study, the chamber was arranged for fifteen, twelve, ten, eight, and five trays equally spaced from each other. The trays were constructed with an anodized aluminum frame and nylon mesh. These are arranged horizontally, with a dimension length (L) of 0.88 m and a width (W) of 0.41 m (Figure 1d).

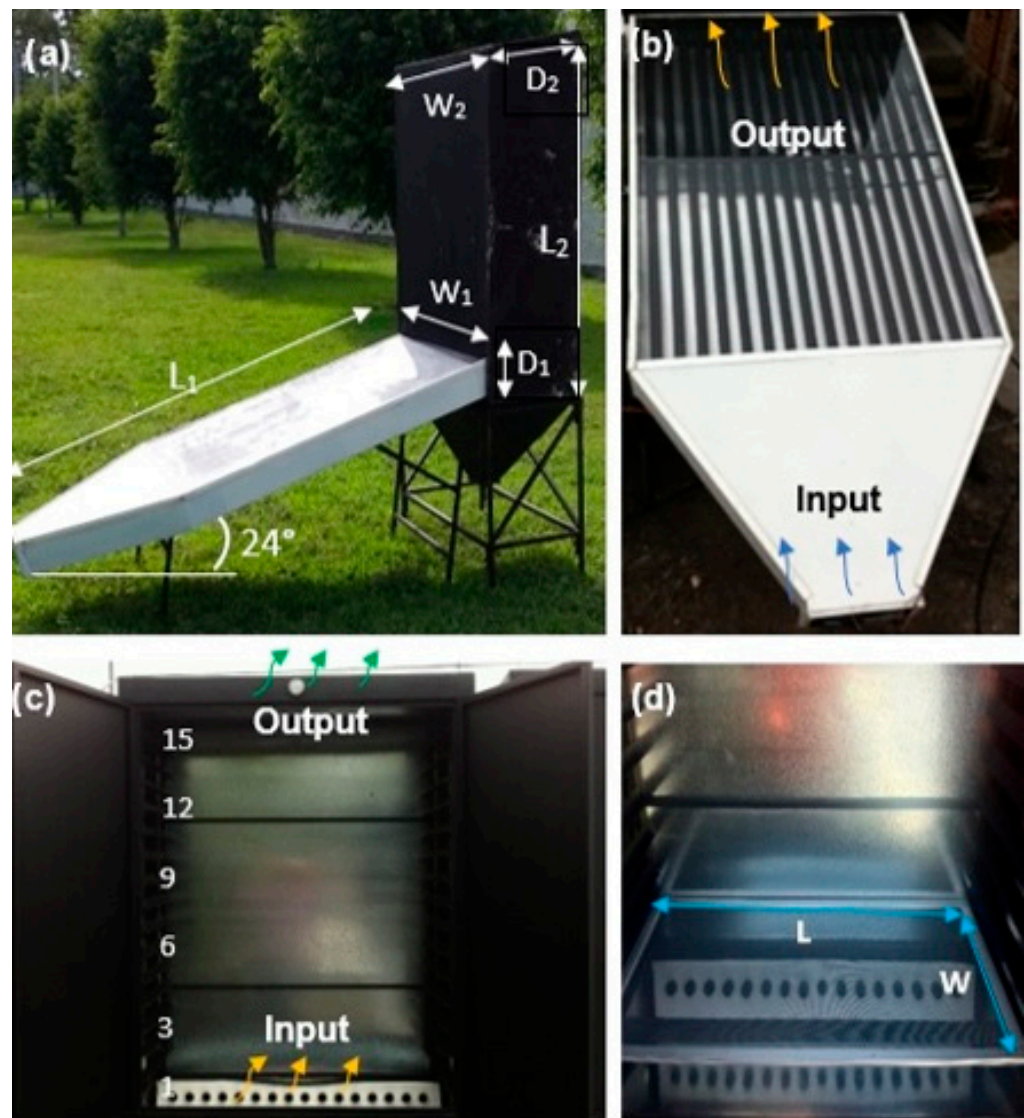


Figure 1. Experimental solar dryer facing south. (a) Exterior view. (b) Airflow ducts of the solar collector. (c) Drying chamber. (d) Trays for drying.

2.2. Data Acquisition

The solar dryer has sensors for the measurement of temperature and airflow velocity. Four of the solar collector's sixteen pipes were designed to contain type K thermocouples with their Max 6675 modules. The sensors are located and represented with S_1 , S_2 , S_3 , and S_4 (Figure 2a). It has a measurement range between $-100\text{ }^{\circ}\text{C}$ to $1250\text{ }^{\circ}\text{C}$. The sensitivity of the sensor is approximately between 41 to $42\text{ }\mu\text{V}/^{\circ}\text{C}$ with an accuracy of $\pm 0.7\text{ }^{\circ}\text{C}$. Likewise, two fans of type NMB with 12 volts and 1.3 ampere operating characteristics were installed at the input of the solar collector (Figure 2a). These were used to supply the airflow to the solar collector and transport the air into the drying chamber. The flow rate was controlled with voltage modules FZ0430 and current modules ACS712. The flow velocity was measured at the input of the drying chamber (see Figure 1c) with a type UT363 anemometer. The measurement range is 0 to $30\text{ }\frac{\text{m}}{\text{s}}$ with a precision of $\pm 5\%$ rdg + 0.5 (Figure 2a). Also, the drying chamber was fitted with a DHT22 (S_5) temperature sensor with a precision of $\pm 0.1\text{ }^{\circ}\text{C}$ (Figure 2b).

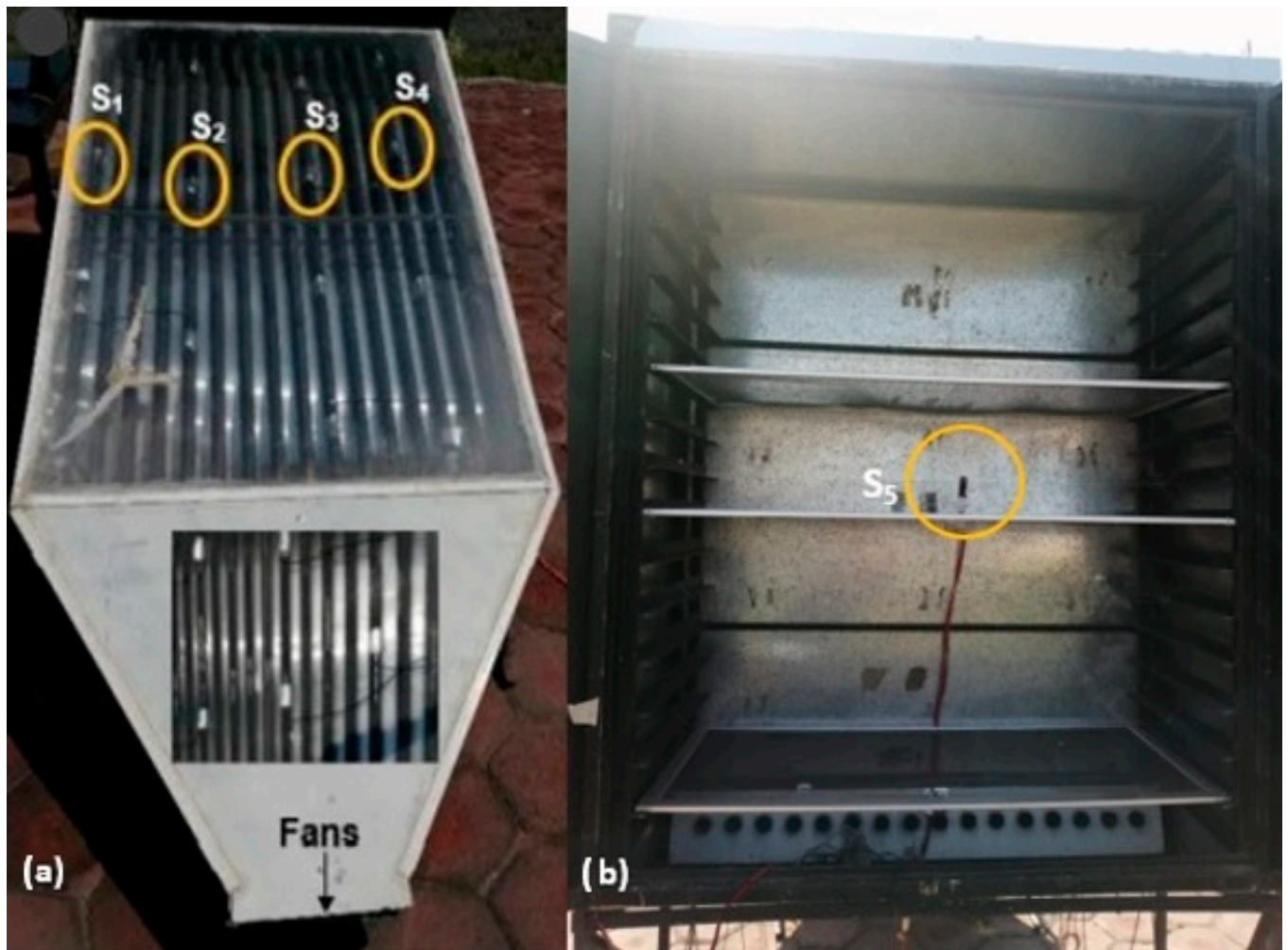


Figure 2. Arrangement of the solar dryer. (a) Location of fans, K-type thermocouples, and anemometers in the solar collector. (b) The DHT22 temperature sensors are inside the drying chamber.

On the other hand, a microcontroller (Arduino, Monza, Italy) was used to interconnect the temperature and humidity sensors and for data acquisition. The microcontroller is connected to a personal computer through a USB port to acquire data. LabVIEW software allows communication between the Arduino microcontrollers for data recording. LabVIEW was used to manage the intensity of the electrical current and, in turn, control the speed of the airflow supplied by the fans.

2.3. Weather Station

A weather station (Ambient Weather, Chandler, AZ, USA; model WS-2902A) was used to measure weather conditions (Figure 3a). Solar radiation and ambient temperature are taken into consideration for the construction of the predictive model. Temperature sensor specifications correspond to a range between -4.4 and 60 °C and solar radiation between 0 and 120 k Lux ($\frac{W}{mm^2}$, lux, fc). The station was installed at a height of 3.5 m and was located near the solar dryer to provide more accurate data (Figure 3b). The data were acquired and recorded remotely into a personal computer then monitored using a display console.

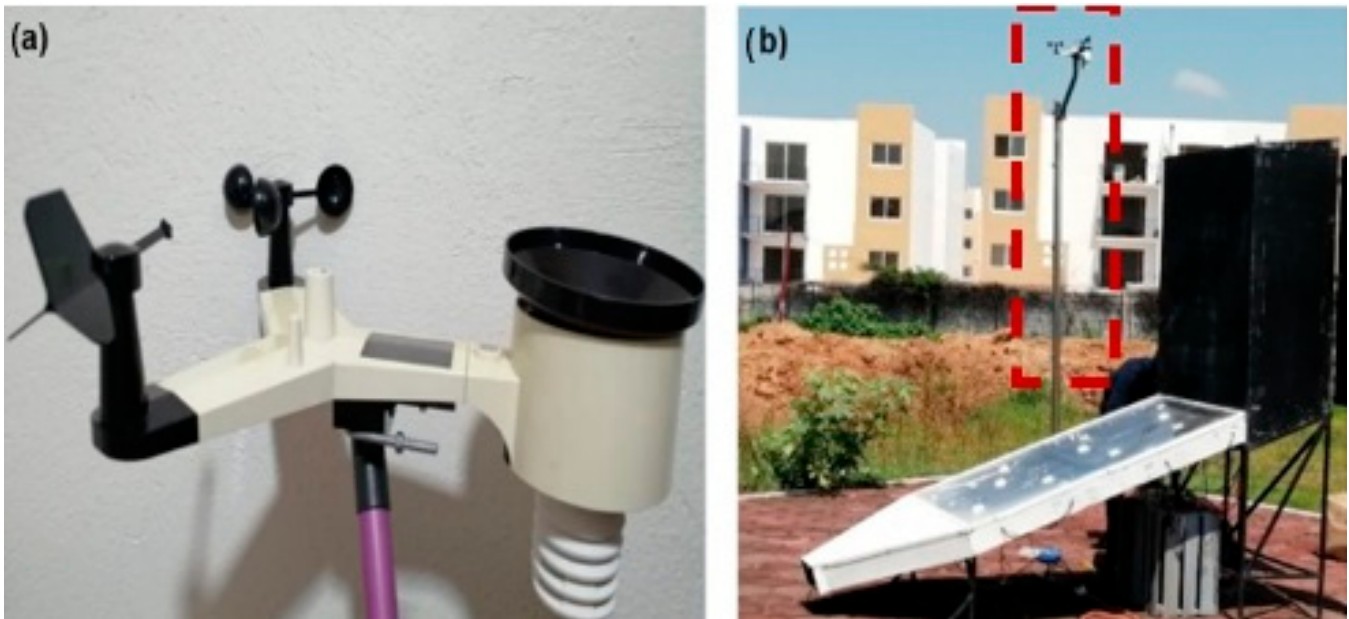


Figure 3. Weather station. (a) Meteorological station for measuring solar radiation and ambient temperature. (b) A 3.5 m high weather station located next to the solar dryer (Red-lined square).

2.4. Artificial Neural Network Model

The method applied is backpropagation, which is used in the training process of forwarding connection networks. Backpropagation is a supervised learning method with a descending gradient: an input pattern propagates through different network layers until it produces an output target. The target is compared to the desired output, and the output neurons calculate the error. The estimated error is transmitted backward from the output layer to the other neurons in the hidden layers. It is proportional to its contribution to the total error of the artificial neural network. With this, the mistakes of the synaptic weights of each neuron used are adjusted.

The input neurons correspond to the first layer, while the intermediate layer is the hidden layer. However, multilayer networks can use the tan-sigmoid (tansig) transfer function. For the last layer, output neurons with linear transfer functions (purelin) are used. Thus, these network outputs can take any value without being limited.

The input vectors normalize between 0.1 and 0.9 due to the tan-sigmoid and purelin transfer function constraints for the hidden and output layers. The transfer function [41] and the normalization equation [42] are given by Equations (1) and (2), respectively.

$$g(x) = \frac{[1 + \tanh(x)]}{2} \quad (1)$$

$$X_i = 0.8 \left(\frac{X_i - X_{min}}{X_{max} - X_{min}} \right) + 0.1 \quad (2)$$

X_i is the value to be normalized; X_{max} is the maximum value; X_{min} the minimum value of the data set.

In this work, the Levenberg–Marquardt (trainlm) algorithm of multilayer backpropagation was used to evaluate the performance of different configurations of the neural network architecture to determine the ideal. Once the backpropagation training algorithm of the multilayer network is known, the architecture is arranged for four layers. The first layer corresponds to the input neurons and a neuron in the output layer. However, due to the complexity and non-linearity of the system on its own, two hidden layers are considered. As there is no rigorous way to determine an optimal number of neurons in the hidden layer, the selection results from a compromise between the computational effort

required for ANN training and an estimate of the minimum number of neurons necessary for capturing dynamic behavior. Therefore, the mean square error (MSE) is applied as an indicator of the performance of the training process, Equation (3) [42]. In this way, it is possible to obtain the ideal architecture for the verification and validation process of the predictive model.

$$SE = \frac{\sum_{i=1}^{i=N} (y_{i,pred} - y_{i,exp})^2}{N} \quad (3)$$

where N is the total number of data points; $y_{i,pred}$ is the network prediction; $y_{i,exp}$ is the experimental response; and i is an index of data.

The predictive model is built considering nine input parameters and one output parameter defining the system. The neural network's inputs are the following parameters:

- Solar radiation (R_a)
- Airflow velocity (V_a)
- Ambient temperature (T_a)
- Solar collector pipe temperatures ($T_{t1}, T_{t2}, T_{t3}, T_{t4}$)
- Number of trays (N_{tray})
- Separation between each of the trays (D_t)
- Drying chamber temperature (T_c).

The data set available (188), 75%, is used for the training process. At the same time, 23% is separated to validate the training.

3. Results

3.1. Climatic Data and Parameters of the Solar Dryer

This section presents the temperature variables, air velocity, and climatological data described in Section 2. The weather data recording was completed every 10 min, corresponding to a cloudy day on 7 August and a clear and non-cloudy day on 18 August 2020. The recording time on 7 August corresponds to approximately between the 12:10 and 2:00 pm hours of the day (central Mexico time). Meanwhile, for the 18th, it fits a schedule approximately between 11:30 am and 2:30 pm. These established schedules have been considered to capture solar radiation as much as possible with the solar dryer.

The following figures present the experimental time series. Figure 4 shows the time series of solar radiation (S_{R1} and S_{R2}) and air temperature (T_{a1} and T_{a2}). Meanwhile, Figure 5 shows the airflow velocity (V_{a1} and V_{a2}). However, the pipe and air temperatures inside the drying chamber are recorded each 1 min over the specified time. Figure 6 shows the temperatures of the pipes, T_{t1} , T_{t2} , T_{t1v} , and T_{t2v} , and the drying chamber, T_c and T_{cv} . Also, Figure 7 presents the temperatures of the pipes: T_{t3} , T_{t4} , T_{t3v} , and T_{t4v} . S_{R1} , T_{a1} , V_{a1} , T_{t1} , T_{t2} , T_{t3} , T_{t4} , and T_c correspond to the data recorded on 18 August. S_{R2} , T_{a2} , V_{a2} , T_{t1v} , T_{t2v} , T_{t3v} , T_{t4v} , and T_{cv} correspond to the data of 7 August. Each of the variables shows disturbances throughout the trajectory. These disturbances are associated with the presence of experimental noise. Figures 6 and 7 also offer the smooth course of each time series. Smoothing makes it possible to reveal meaningful patterns in our data while omitting the contribution of noise. Here, a moving average filter has been applied. Figure 6 shows pipe temperatures: T_{t1s} , T_{t2s} , T_{t1vs} , and T_{t2vs} , and the drying chamber: T_{cs} and T_{cvs} . Figure 7 presents pipe temperatures: T_{t3s} , T_{t4s} , T_{t3vs} , and T_{t4vs} .

Table 1 shows the essential parameters of the solar dryer geometry to construct the neural network model to predict the temperature inside the drying chamber. The predictive model can provide the chamber temperature for different numbers of symmetrically separated trays. For this, three arrays of the number of trays (N_{tray}) with their respective separation distances (D_t) are used in training and verifying the model. For the validation, five tray arrangements are considered; see Table 1.

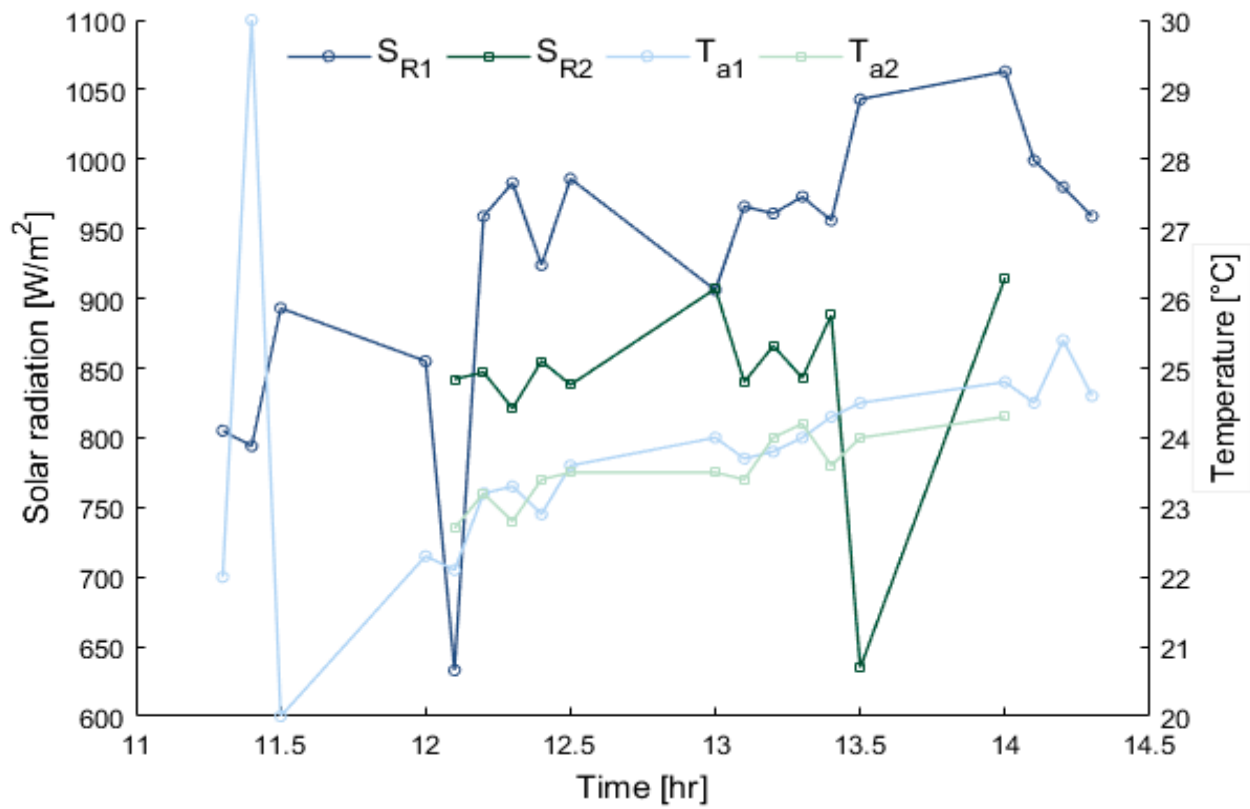


Figure 4. Solar radiation time series and air temperature time series. S_{R1} and T_{a1} are data recorded on 18 August. S_{R2} and T_{a2} are data recorded on 7 August.

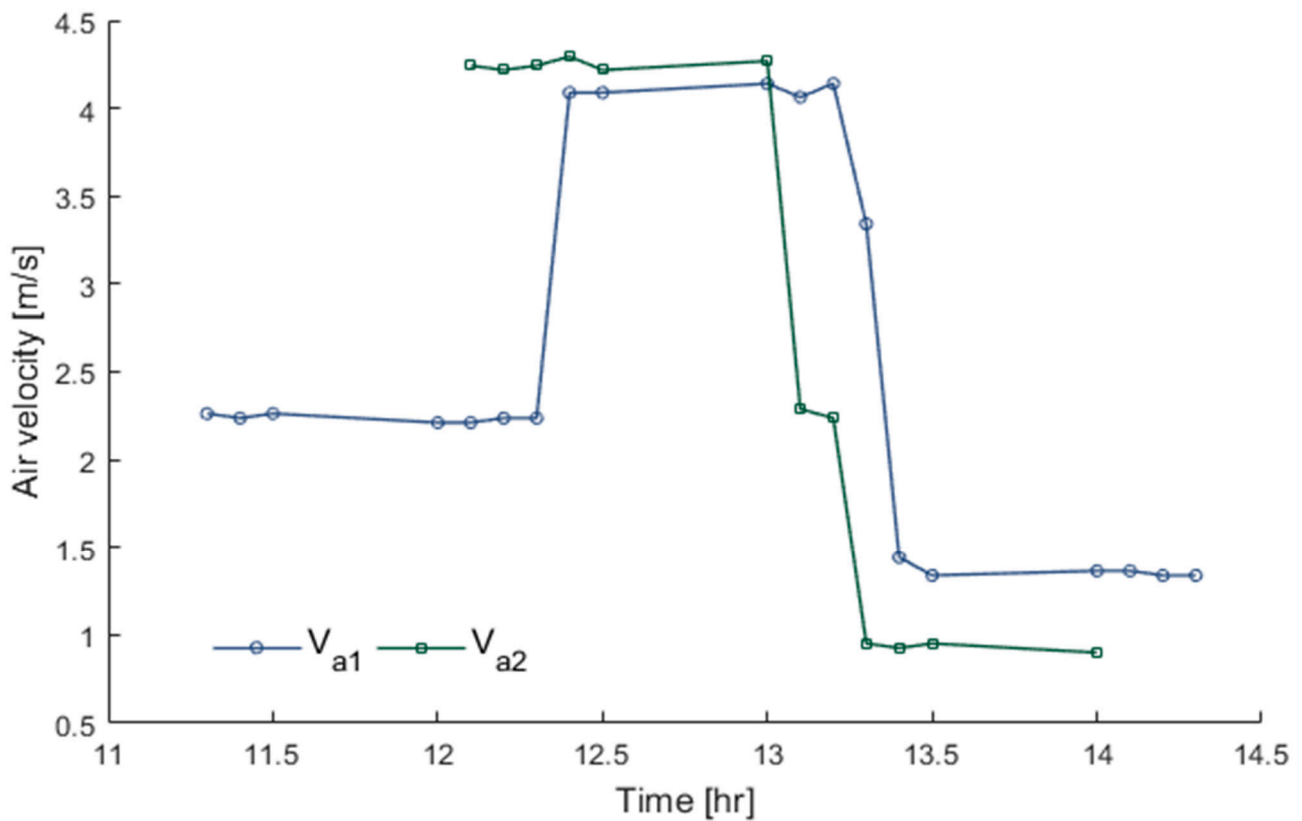


Figure 5. Airflow velocity time series. V_{a1} and V_{a2} data are recorded on 7 and 18 August, respectively.

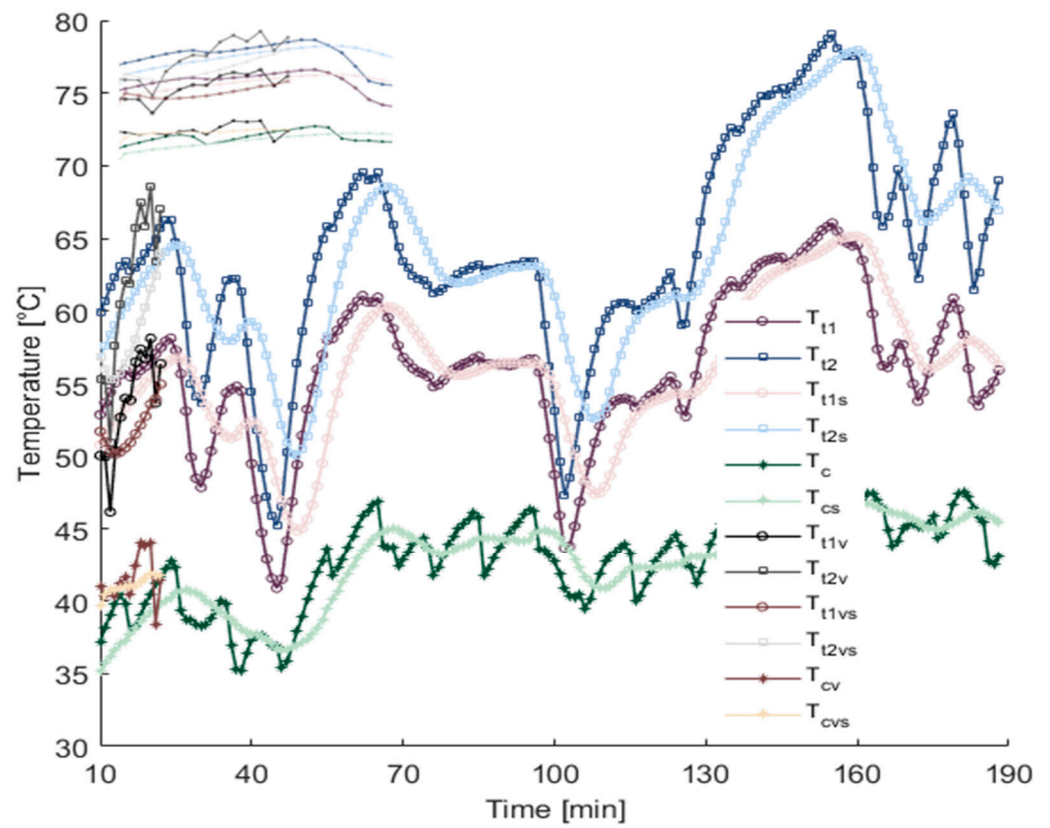


Figure 6. Pipe temperature time series. Experimental: T_{t1} , T_{t2} , T_{t1v} , T_{t2v} , T_c , and T_{cv} versus smoothed: T_{t1s} , T_{t2s} , T_{t1vs} , T_{t2vs} , T_{cs} , and T_{cvs} .

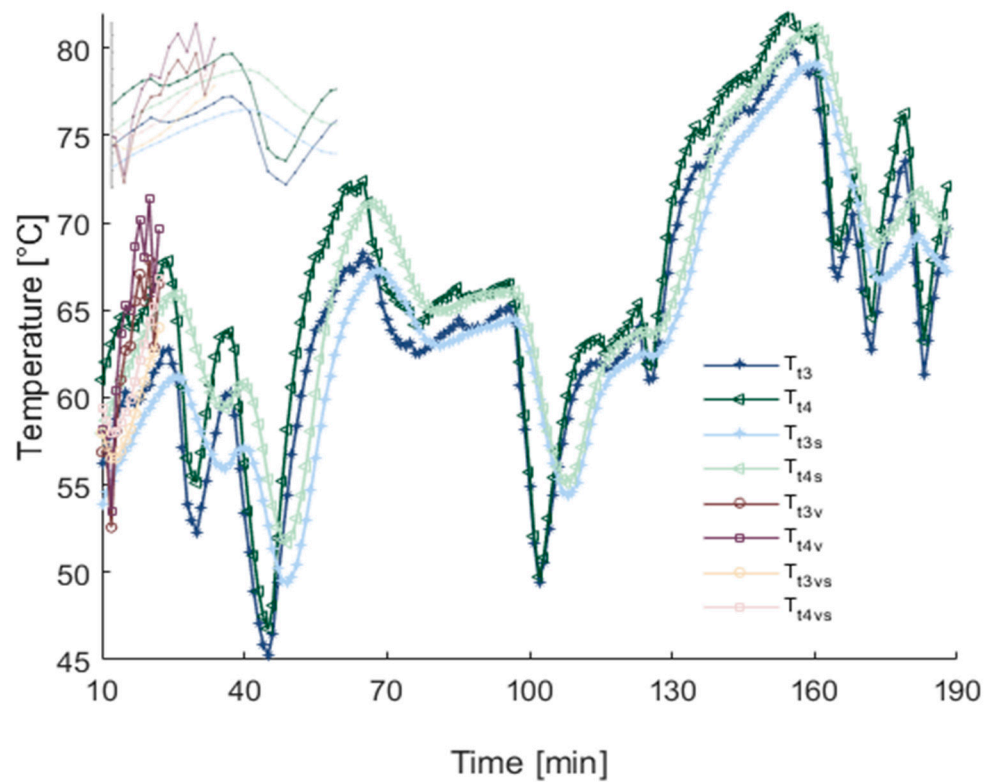


Figure 7. Pipe temperature time series. Experimental ones: T_{t3} , T_{t4} , T_{t3v} , and T_{t4v} vs. smoothed: T_{t3s} , T_{t4s} , T_{t3vs} , and T_{t4vs} .

Table 1. Drying chamber configuration.

Training–Verification		Validation	
(N_{tray})	$D_t (m)$	(N_{tray})	$D_t (m)$
15	0.07	15	0.07
10	0.105	12	0.087
5	0.21	10	0.105
		8	0.131
		5	0.21

3.2. Results of the Artificial Neural Network

According to the linear regression statistical modeling technique, the backpropagation algorithms were evaluated using the multiple determination coefficients (R^2) and the mean square error (MSE) criteria. The equation obtained with the linear regression minimized the distance between a fit line for experimental and predicted data points in the training process. This technique describes a continuous response variable as a function of one or more predictor variables [43–45]. The algorithm with the best performance was Levenberg–Marquardt (trainlm), with an R^2 of 0.94162 and an MSE of 0.9725. This last algorithm is used to conduct the training and prediction process and select the number of neurons within each hidden layer.

No technique or methodology exists to determine the optimal number of neurons within the hidden layers, as mentioned in Section 2.4. However, some authors recommend conducting a study for the calculation [46–48]. Therefore, the maximum number of neurons obtained is based on the trade-off between the computational effort required during the training process of the ANN and the estimate of the minimum number of neurons needed. On the other hand, an approximation is made through the geometric pyramid rule to start from an initial number of neurons in the hidden layers until the ideal is obtained. The trial-and-error phase is carried out from this process to find the best performance for the prediction process. In this training process, 75% of the data set (188) was used, while the rest was used for model verification. The criterion for obtaining the number of neurons in the hidden layers was based on the deviations used to obtain the architecture's configuration (MSE). According to performance analysis and the MSE estimation during the training process of the ANN, the best network configuration was 9-13-12-1, with an MSE below 1%. Therefore, the ANN configuration verifies and validates the model (see Figure 8).

3.3. Verification and Validation of Results

The verification and validation of the artificial neural network model for predicting the temperature in the drying chamber are shown in this section. Likewise, the relative error between the experimental and predicted data is also shown.

Forty-seven data points, from one hundred eighty-eight of 18 August 2020, were considered for verifying the predictive model. Figure 9 presents the results of the temperature prediction between the predicted (T_{ANN}) and experimental (T_{exp}) data from the drying chamber. Here, neural network results follow the trajectory throughout the trend, trying to resemble the experimental data. The relative error between the predicted and observed data is below 0.25% (see Figure 10). The error calculated makes the model reliable for making predictions with similar conditions to those proposed. For this, the neural network model is validated with a set of 24 data points.

However, for the validation process of the same model, 24 data points from 7 August 2020, of that same year, are considered. Figure 11 shows the validation results of the ANN model. Again, the neural network predicts data very close to the experimental values. The estimated relative error is below 0.25% (Figure 10).

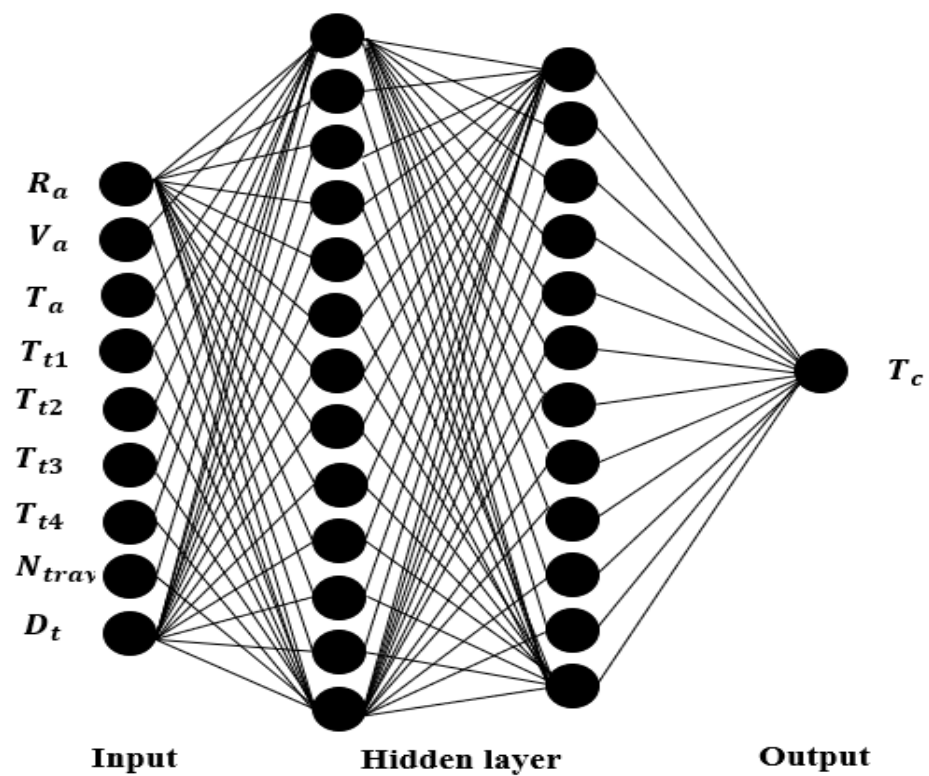


Figure 8. The architecture of the artificial neural network. The configuration is nine neurons in the input layer, two hidden layers with thirteen and twelve neurons, and one in the output layer (9-13-12-1). The parameters are solar radiation (R_a), airflow velocity (V_a), ambient temperature (T_a), temperatures in tube 1 (T_{t1}), temperatures in tube 2 (T_{t2}), temperatures in tube 3 (T_{t3}), temperatures in tube 4 (T_{t4}), number of trays (N_{tray}), the separation between each of the trays (D_t), and the temperature in the drying chamber (T_c).

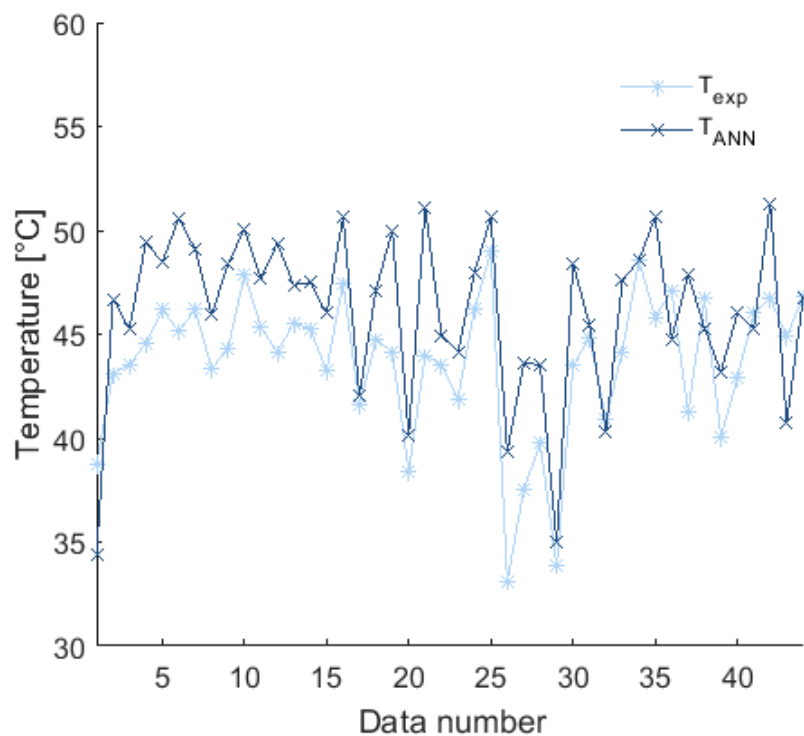


Figure 9. Predicted temperatures (T_{ANN}) vs. experimental temperatures (T_{exp}) of the model verification.

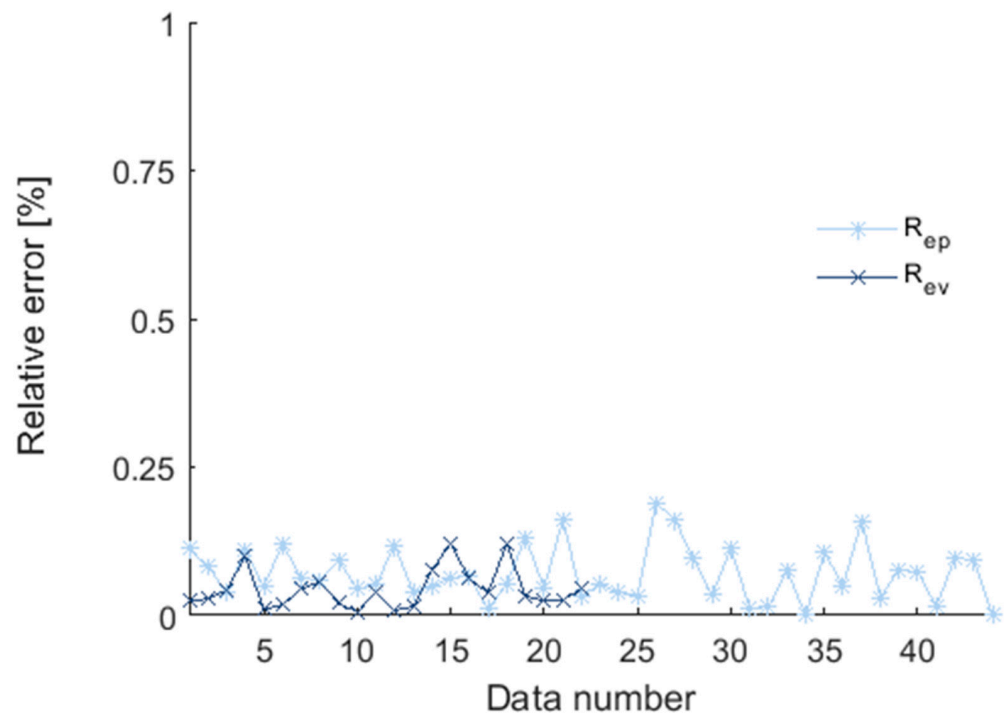


Figure 10. Relative error between predicted vs. experimental data. R_{ep} relative error for verification. R_{ev} relative error for validation.

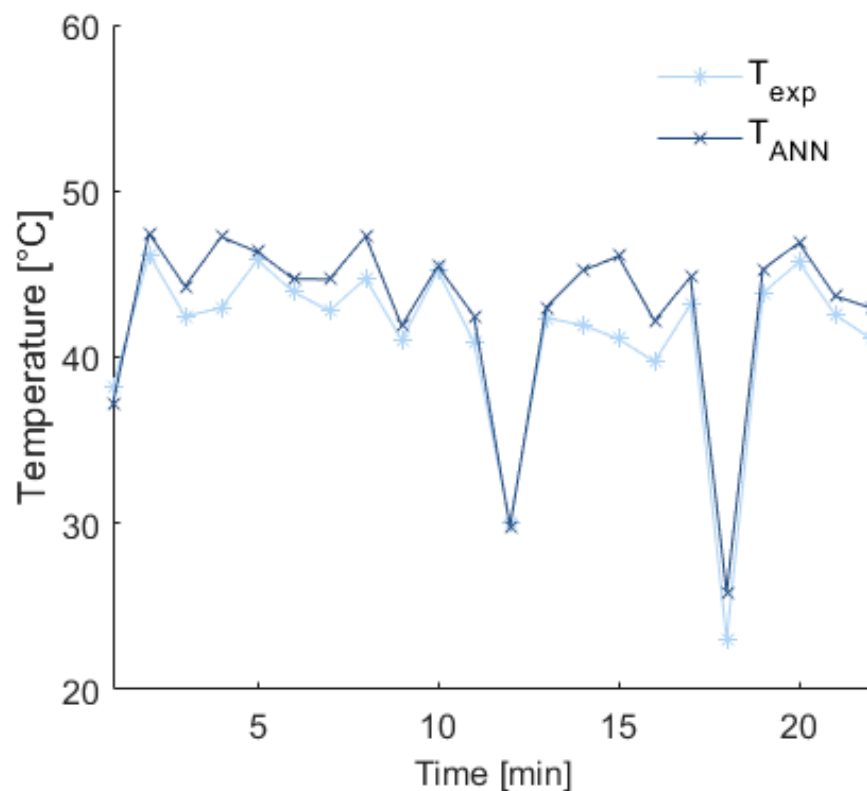


Figure 11. Predicted temperatures (T_{ANN}) vs. experimental temperatures (T_{exp}) of the model validation.

4. Discussion

The temperature inside the chamber plays a vital role in the drying process. The importance lies in the determining factor of temperature prediction, which correlates with how much heat the solar dryer can provide for drying. However, time is an important

parameter that needs to be known; a future study should consider the type and quantity of products. Therefore, in this work, the drying chamber temperatures are predicted to help investigate a future model that involves the type and amount of product to be dried based on its moisture content. Likewise, raising the chamber's temperature allows the humidity of the air to be reduced through the ducts of the solar collector to be transported into the chamber. The ideal temperature for drying vegetables, fruits, and meats, among others, is between 30 and 70 °C [10,11,15,16,38,49]. Obtaining lower temperatures would cause the decomposition of the product subjected to drying due to the proliferation of microorganisms. When the temperature exceeds 70 °C, the product subjected to drying may exhibit degradation of its functional compounds [11,50]. Maintaining the temperature in solar dryers is a complex problem due to the variable weather conditions.

For our study, weather conditions, pipe temperatures, the air temperature in the drying chamber, and the speed of the airflow supplied to the solar collector were correctly recorded. Due to the noise present in each variable, these were smoothed through the moving average filter technique to create the neural network model. The smoothing of the data allowed the development of the predictive model of the network. Different neural network configurations were proposed, and the best structure determined was 9-13-12-1. The neural network model's capabilities were tested, and the verification was performed for an experimental data set. The model presented good predictive capabilities, obtaining relative errors below 0.25%. This type of error makes the model reliable with other weather conditions if they are within the range of conditions established in model training. The model was validated with experimental data for the same variables and input parameters for another specific day from 12:10 to 14:00. Again, the response was favorable as the prediction results closely followed the experimental trajectory, with an error like the verification.

The predictive model of the neural network has once again demonstrated its viability with similar conditions that have been applied for another time of year. It should be noted that this model can replace traditional models that use computational and experimental numerical models [6–13] to analyze thermal behavior in solar dryers, which become tedious due to the number of variables involved and the geometric shapes for their study. However, one of the essential advantages of this model is that it provides better predictive capabilities without considering the complexity of the system but considering the variables of interest that allow us to know its behavior. This model could be a basis for developing a real-time optimization tool for the operation and optimal design of indirect solar dryers involving the type, quantity, and moisture content of the product to be dried.

The solar dryer design for this case study uses radiant energy to raise the airflow temperature through the collector and transport it by a forced medium toward the chamber, reaching a temperature between 40 to 50 °C for different quantities of trays inside the drying chamber.

5. Conclusions

An indirect solar dryer has been presented to know the system's dynamics. Weather conditions, airflow velocities, ambient temperature, and solar collector piping have been successfully recorded. A configuration of five trays in the drying chamber was proposed to determine the temperature behavior.

A feed-forward neural network trained with the Levenberg–Marquardt (trainlm) algorithm showed good predictive capabilities. This algorithm was used to determine the ideal configuration of the network architecture. The network configuration was obtained for nine neurons in the input layer, one in the output layer, and two hidden layers of thirteen and twelve neurons each (9-13-12-1), with an MSE error of 0.9725. This configuration reduced the cost and time of the network learning process.

The predictive model was successfully tested, achieving a good predictor for forecasting the air temperature inside the drying chamber. It is reflected when the relative

error between predicted and experimental temperatures is obtained. The relative error was below 0.25% for the model's verification and validation.

In addition, this model could serve as a basis for developing a real-time optimization tool for the operation and optimal design of indirect solar dryers. However, other factors must be considered, such as extreme weather conditions, low or high temperatures, and the type, quantity, and moisture content of the product to be dried.

Author Contributions: Conceptualization, A.T.B. and R.R.M.; methodology, A.T.B., R.R.M. and E.C.L.-V.; software, A.T.B. and C.T.S.; validation, A.T.B., R.R.M. and E.M.P.; formal analysis, A.T.B. and R.R.M.; investigation, A.T.B.; resources, A.T.B. and J.L.G.P.; data curation, A.T.B. and E.C.L.-V.; writing—original draft preparation, A.T.B. and R.R.M.; writing—review and editing, A.T.B., R.R.M. and C.T.S.; visualization, A.T.B. and E.M.P.; supervision, A.T.B., R.R.M. and J.L.G.P.; project administration, A.T.B. and R.R.M. All authors have read and agreed to the published version of the manuscript.

Funding: This research received no external funding.

Data Availability Statement: No new data were created or analyzed in this study. Data sharing is not applicable to this article.

Conflicts of Interest: The authors declare no conflict of interest.

References

1. Tlatelapa-Becerro, A.; Rico-Martínez, R.; Urquiza, G.; Calderón-Ramírez, M. Obtaining of *Crataegus mexicana* leaflets using an indirect solar dryer. *Rev. Mex. Ing. Quím.* **2020**, *2*, 669–676. [[CrossRef](#)]
2. Marwan, B.; Chawki, L.; Mirna, F.L.; Christy, L. Solar drying simulation of different products: Lebanese case. *Energy Rep.* **2020**, *6*, 548–564. [[CrossRef](#)]
3. Abhay, L.; Chandramohan, V.P.; Raju, V.R.K. Design, Development and Performance of Indirect Type Solar Dryer for Banana Drying. *Energy Procedia* **2017**, *109*, 409–416. [[CrossRef](#)]
4. Kokatea, D.H.; Kale, D.M.; Korpale, V.S.; Shinde, Y.H.; Panse, S.V.; Deshmukh, S.P.; Pandit, A.B. Energy Conservation Through Solar Energy Assisted Dryer for Plastic Processing Industry. *Energy Procedia* **2014**, *54*, 376–388. [[CrossRef](#)]
5. Nabnean, S.; Nimnuan, P. Experimental performance of direct forced convection household solar dryer for drying banana. *Case Stud. Therm. Eng.* **2020**, *22*, 100787. [[CrossRef](#)]
6. Elieser, T. Mathematical modeling and simulation of a solar agricultural dryer with back-up biomass burner and thermal storage. *Case Stud. Therm. Eng.* **2018**, *12*, 149–165. [[CrossRef](#)]
7. Mehmet, D.; Erdem, A.; Ebru, K.A. Numerical and experimental analysis of heat and mass transfer in the drying process of the solar drying system. *Eng. Sci. Technol. Int. J.* **2021**, *24*, 236–246. [[CrossRef](#)]
8. Petros, D.; Mesele, H.; Amanuel, K.; Asfaw, H.; Mekonnen, G.; Maarten, V. Design, development and CFD modeling of indirect solar food dryer. *Energy Procedia* **2019**, *158*, 1128–1134. [[CrossRef](#)]
9. Guofeng, Y.; Liang, H.; Xing, L.; Li, X.; Wenxue, T.; Zhifeng, W. Experimental investigation of a solar dryer system for drying carpet. *Energy Procedia* **2018**, *70*, 626–633. [[CrossRef](#)]
10. Nimnuan, P.; Nabnean, S. Experimental and simulated investigations of the performance of the solar greenhouse dryer for drying cassumunar ginger (*Zingiber cassumunar* Roxb.). *Case Stud. Therm. Eng.* **2020**, *22*, 100745. [[CrossRef](#)]
11. Mohammed, A.H.; Klaus, G.; Mohammad, S.H. Mathematical model for a heat pump dryer for aromatic plant. *Procedia Eng.* **2013**, *56*, 510–520. [[CrossRef](#)]
12. Hosain, D.; Abbas, R.A.; Ali, A.; Mohsen, A.; Gholamhassan, N.; Jalal, K. Study of the drying kinetics of pepper. *J. Saudi Soc. Agric. Sci.* **2014**, *13*, 130–138. [[CrossRef](#)]
13. Mourad, A.; Salah, B.M.; Imed, Z.; Ahmed, B. Kinetic study of the convective drying of spearmint. *J. Saudi Soc. Agric. Sci.* **2014**, *13*, 1–7. [[CrossRef](#)]
14. Oluwole, A.O.; Oluyemisi, A.A.; Pelumi, E.O.; Hilary, I.O.; Adebowale, O.A.; Esivue, A.S. Drying kinetic of industrial cassava flour: Experimental data in view. *Data Brief* **2017**, *15*, 501–510. [[CrossRef](#)]
15. Ramallo, L.A.; Mascheroni, R.H. Quality evaluation of pineapple fruit during drying process. *Food Bioprod. Process.* **2012**, *90*, 275–283. [[CrossRef](#)]
16. Shiva, K.M.; DurgaPrasad, B.; Basavaraj, M. An Experimental Study on Drying Kinetics of Guava Fruit (*Psidium guajava* L.) By Thin Layer Drying. *IOSR J. Environ. Sci. Toxicol. Food Technol.* **2015**, *1*, 74–80.
17. Tlatelapa, B.A.; Rico, M.R.; Castro, G.L.; Urquiza, G.; Calderón-Ramírez, M. Artificial Neural Networks (ANN) and Kalman Filter Algorithms to Predict Output Temperatures on a Heat Exchanger. *Int. J. Appl. Eng. Res.* **2018**, *17*, 13130–13135.
18. Hikmet, E.; Mustafa, I. Modelling of a vertical ground coupled heat pump system by using artificial neural networks. *Expert Syst. Appl.* **2009**, *36*, 10229–10238. [[CrossRef](#)]

19. González, G.R.; Rico, M.R.; Wolf, W.; Lübke, M.; Eiswirth, M.; Anderson, J.S.; Kevrekidis, I.G. Characterization of a two-parameter mixed-mode electrochemical behavior regime using neural networks. *Phys. D Nonlinear Phenom.* **2001**, *151*, 27–43. [[CrossRef](#)]
20. Kapil, V.; Panigrahy, P.K. Artificial neural network control of a heat exchanger in a closed flow air circuit. *Appl. Soft Comput.* **2005**, *5*, 441–465. [[CrossRef](#)]
21. Ramírez, A.E.; Calderon, R.M.; Rico, M.R.; Gonzalez, F.C.; Parmananda, P. Detecting Bifurcations in an Electrochemical Cell Employing an Assisted Reference Model Strategy. *J. Phys. Chem.* **2012**, *117*, 535–540. [[CrossRef](#)]
22. Hikmet, E.; Mustafa, I.; Abdulkadir, S.; Mehmet, E. Performance prediction of a ground-coupled heat pump system using artificial neural networks. *Expert Syst. Appl.* **2008**, *35*, 1940–1948. [[CrossRef](#)]
23. Vinoth, K.K.; Paradeshi, L.; Srinivas, M.; Jayaraj, S. Parametric Studies of a Simple Direct Expansion Solar Assisted Heat Pump Using ANN and GA. *Energy Procedia* **2016**, *90*, 625–634. [[CrossRef](#)]
24. Luca, S.; Herbert, A.Z.; Jan, D.; Camilo, C.M.; Van Bael, J.; Adriano, S. Modeling the performance of a sorption thermal energy storage reactor using artificial neural networks. *Appl. Energy* **2019**, *253*, 113525. [[CrossRef](#)]
25. Ashly, M.T.; Nizar, A.; Subathra, M.S.; Lazarus, G.A. Analysing the Performance of a Flat Plate Solar Collector with Silver/Water Nanofluid Using Artificial Neural Network. *Procedia Comput. Sci.* **2016**, *93*, 33–40. [[CrossRef](#)]
26. Chaibi, Y.; Malvoni, M.; El, R.T.; Kousksou, T.; Zeraoui, Y. Artificial neural-network based model to forecast the electrical and thermal efficiencies of PVT air collector systems. *Clean. Eng. Technol.* **2021**, *4*, 100132. [[CrossRef](#)]
27. Gilles, N.; Christophe, P.; Said, D. Estimation of tilted solar irradiation using Artificial Neural Networks. *Energy Procedia* **2013**, *42*, 33–42. [[CrossRef](#)]
28. İlhan, C.; Okan, E.; Engin, G.; Ali, E.G. The prediction of photovoltaic module temperature with artificial neural networks. *Case Stud. Thermal Eng.* **2014**, *3*, 11–20. [[CrossRef](#)]
29. Anurag, K.; Nikhil, R.; Pijush, S. Prediction of heat transfer rate of a Wire-on-Tube type heat exchanger: An Artificial Intelligence approach. *Procedia Eng.* **2013**, *64*, 74–83. [[CrossRef](#)]
30. Haritonova, L. On Neural Modeling of Heat Exchange in Heat Exchangers (Recuperators) with the Systems of Plane-Parallel Impingement Jets for Machine Building and Metallurgical Productions. *Procedia Eng.* **2017**, *206*, 1002–1008. [[CrossRef](#)]
31. Promvong, P.; Eiamsa, A.S.; Wongcharee, K.; Chuwattanakul, V.; Samruaisin, P.; Chokphoemphun, S.; Nanan, K.; Eiamsa, A.P. Characterization of heat transfer and artificial neural networks prediction on overall performance index of a channel installed with arc-shaped baffle turbulators. *Case Stud. Therm. Eng.* **2021**, *26*, 101067. [[CrossRef](#)]
32. Xie, G.N.; Wang, Q.W.; Zeng, M.; Luo, L.Q. Heat transfer analysis for shell-and-tube heat exchangers with experimental data by artificial neural networks approach. *Appl. Therm. Eng.* **2007**, *27*, 1096–1104. [[CrossRef](#)]
33. Yasar, I. A new approach for the prediction of the heat transfer rate of the wire-on-tube type heat exchanger—use of an artificial neural network model. *Appl. Therm. Eng.* **2003**, *23*, 243–249. [[CrossRef](#)]
34. Gabriele, B.; Vincenzo, T.; Nadia, U. Neural Networks Implementation for Analysis and Control of Heat Exchange Process in a Metal Foam Prototypal Device. *Procedia CIRP* **2017**, *62*, 518–522. [[CrossRef](#)]
35. Gupta, A.K.; Kumara, P.; Sahoo, R.K.; Sahub, A.K.; Sarangia, S.K. Performance measurement of plate fin heat exchanger by exploration: ANN, ANFIS, GA, and SA. *J. Comput. Des. Eng.* **2017**, *4*, 60–68. [[CrossRef](#)]
36. Yasar, I.; Akif, K.; Cem, P. Performance prediction for non-adiabatic capillary tube suction line heat exchanger: An artificial neural network approach. *Energy Convers. Manag.* **2005**, *46*, 223–232. [[CrossRef](#)]
37. Mohammad, K.; Vali, R.S.; Reza, A.C.; Ebrahim, T.; Abbaspour, G.Y.; Iman, G. ANFIS and ANNs model for prediction of moisture diffusivity and specific energy consumption potato, garlic and cantaloupe drying under convective hot air dryer. *Inf. Process. Agric.* **2018**, *5*, 372–387. [[CrossRef](#)]
38. Momenzadeh, L.; Zomorodian, A.; Mowla, D. Applying Artificial Neural Network for Drying Time Prediction of Green Pea in a Microwave Assisted Fluidized Bed Dryer. *J. Agr. Sci. Technol.* **2012**, *14*, 513–522. [[CrossRef](#)]
39. Shamsollah, A.; Kosari, M.A.; Mohammad, B. Prediction of wheat moisture content at harvest time through ANN and SVR modeling techniques. *Inf. Process. Agric.* **2020**, *7*, 500–510. [[CrossRef](#)]
40. Tohsing, K.; Janjai, S.; Lamlert, N.; Mundpookhier, T.; Chanalert, W.; Bala, B.K. Experimental performance and artificial neural network modeling of solar drying of litchi in the parabolic greenhouse dryer. *J. Renew. Energy Smart Grid Technol.* **2018**, *13*, 83–95.
41. Krischer, K.; Rico, M.R.; Kevrekidis, I.G.; Rotermund, H.H.; Ertl, G.; Hudson, J.L. Model identification of a spatiotemporally varying catalytic reaction. *AIChE J.* **1993**, *1*, 89–98. [[CrossRef](#)]
42. Khataee, A.R.; Kasiri, M.B. Artificial neural networks modeling of contaminated water treatment processes by homogeneous and heterogeneous nanocatalysis. *J. Mol. Catal. A Chem.* **2010**, *331*, 86–100. [[CrossRef](#)]
43. Arzu, S.S. Performance analysis of single-stage refrigeration system with internal heat exchanger using neural network and neuro-fuzzy. *Renew. Energy* **2011**, *36*, 2747–2752. [[CrossRef](#)]
44. Jian, Z.; Fariborz, H. Development of Artificial Neural Network based heat convection algorithm for thermal simulation of large rectangular cross-sectional area Earth-to-Air Heat Exchangers. *Energy Build.* **2010**, *42*, 435–440. [[CrossRef](#)]
45. Reza, B.; Masoud, R. Prediction of heat transfer and flow characteristics in helically coiled tubes using artificial neural networks. *Int. Commun. Heat Mass Transf.* **2012**, *39*, 1279–1285. [[CrossRef](#)]
46. Gongnan, X.; Bengt, S.; Qiuwang, W.; Linghong, T. Performance predictions of laminar and turbulent heat transfer and fluid flow of heat exchangers having large tube-diameter and large tube-row by artificial neural networks. *Int. J. Heat Mass Transf.* **2009**, *52*, 2484–2497. [[CrossRef](#)]

47. Soheil, A.; Carey, J.S.; Robert, W.B. Application of neural networks to predict the transient performance of a Run-Around Membrane Energy Exchanger for yearly non-stop operation. *Int. J. Heat Mass Transf.* **2012**, *55*, 5403–5416. [[CrossRef](#)]
48. Unal, A.; Aydin, K.M.; Feridun, O.A. Estimation of heat transfer in oscillating annular flow using artificial neural networks. *Adv. Eng. Softw.* **2009**, *40*, 864–870. [[CrossRef](#)]
49. Romero, V.M.; Cerezo, E.; Garcia, M.; Sanchez, M.H. Simulation and validation of vanilla drying process in an indirect solar dryer prototype using CFD Fluent program. *Energy Procedia* **2014**, *57*, 1651–1658. [[CrossRef](#)]
50. Suherman, S.; Hadiyanto, H.; Evan, E.S.; Shesar, A.R.; Aditya, R.P. Towards an optimal hybrid solar method for lime-drying behavior. *Heliyon* **2020**, *6*, e05356. [[CrossRef](#)] [[PubMed](#)]

Disclaimer/Publisher's Note: The statements, opinions and data contained in all publications are solely those of the individual author(s) and contributor(s) and not of MDPI and/or the editor(s). MDPI and/or the editor(s) disclaim responsibility for any injury to people or property resulting from any ideas, methods, instructions or products referred to in the content.